PUBLICATIONS OF THE ASTRONOMICAL SOCIETY OF THE PACIFIC, **110**:165–185, 1998 February

Adaptive Optics Sky Coverage Calculations for the Gemini-North Telescope

B. L. ELLERBROEK

Starfire Optical Range, USAF Research Laboratory, Kirtland AFB, NM 87117; ellerbrb@ug2.plk.af.mil

AND

D. W. TYLER

Schafer Corporation, Kirtland AFB, NM 87117; tyler@freestyle.plk.af.mil

Received 1997 July 24; accepted 1997 November 15

ABSTRACT. Sky coverage results are presented for several natural guide star (NGS) and laser guide star (LGS) adaptive optics (AO) configurations using scenario, telescope, and AO design parameters derived from the Gemini-North 8 m telescope. "Sky coverage" is defined as that fraction of the sky over which the AO system provides a useful level of performance, in this case a high Strehl ratio in the *J*, *H*, or *K* band. Some of the factors considered in this study include optimization of the AO wavefront reconstruction algorithm and control bandwidth, the effect of windshake-induced tip/tilt jitter, and the conjugation of the AO system's deformable mirror (DM) and wavefront sensor (WFS) to the dominant seeing layer at the Gemini-North site. The degree of compensation of the tip/tilt guide star image by the higher order adaptive optics is also considered. LGS AO using a single beacon in the mesospheric sodium layer typically improves sky coverage by about an order of magnitude relative to NGS AO, principally because a very dim natural guide star is sufficient for tip/tilt sensing when its image is sharpened by LGS higher order compensation. The values assumed for windshake, seeing, zenith angle, and the conjugate range of the DM and WFS also have a highly significant effect upon the estimated sky coverage for both the NGS and the LGS AO systems. The first three of these factors will need to be considered by scheduling algorithms for queue-based observing.

1. INTRODUCTION

The potential benefits of adaptive optics (AO) for large, ground-based astronomical telescopes are now becoming apparent through the results obtained with several AO systems (Rigaut et al. 1992; Close et al. 1996; Shelton et al. 1996; Rigaut et al. 1996; Ryan et al. 1996). As the AO systems for large telescopes such as Gemini, Keck, Subaru, and VLT progress toward their eventual commissioning, the task is now to select design approaches and parameters that will maximize system performance and the resulting payoff for the intended scientific applications. One important measure of performance is described by the AO system's sky coverage (Rigaut & Gendron 1992), defined as that fraction of the sky for which the system provides a useful level of atmospheric turbulence compensation. With the exception of observing programs that intrinsically study bright stars themselves suitable for use as wavefront sensing beacons, many proposed studies will benefit from the use of adaptive optics only if the level of sky coverage achieved is relatively large. See Morris et al. (1996) for the significance of high sky coverage for several applications of AO anticipated for the Gemini Project.

Sky coverage is limited for both natural guide star (NGS) and laser guide star (LGS) AO systems owing to anisoplanatism (Fried 1982) and the relative scarcity of stars sufficiently bright for wavefront or tip/tilt sensing. One might intuitively expect that a LGS AO system should provide a increase in sky coverage relative to a NGS AO system, since the former approach requires a natural guide star to correct tip/tilt only instead of the entire turbulence-induced wavefront distortion. Previous calculations (Rigaut & Gendron 1992; Parenti & Sasiela 1994) have indicated that this is indeed the case, at least for fairly generic atmospheric profiles and AO system models. Because of the additional expense and complexity associated with LGS AO, quantifying this advantage for specific sites and AO system design approaches is highly desirable. This paper describes the results of one such study undertaken at the request of the Gemini Project, for which the following considerations require special attention:

1. Sky coverage defined in terms of high Strehl ratios in *J*, *H*, and *K* bands.
2. Atmospheric models corresponding to the Gemini-North site.

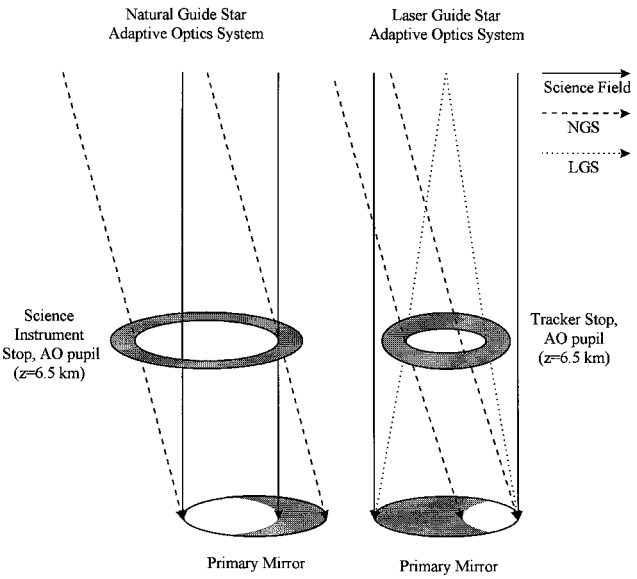

FIG. 1.—Guide star and aperture stop geometries for a nonzero AO conjugate range

3. LGS AO using a single laser guide star in the mesospheric sodium layer.
4. Tip/tilt jitter induced by wind buffeting of the telescope and enclosure (windshake).
5. Tip/tilt sensing at IR wavelengths using a low-order Shack-Hartmann sensor.
6. Wavefront sensing and correction optically conjugate to a range of 6.5 km, the mean altitude of turbulence at the Gemini-North site.

We calculate that the LGS AO system typically increases sky coverage by about an order of magnitude over NGS AO when these factors are included in the analysis. The values assumed for windshake, seeing, zenith angle, and the AO conjugate range also have a very significant effect upon sky coverage for both AO systems.

Section 2 outlines the AO system and scenario parameters used in these calculations. Section 3 illustrates the significance of factors 4–6 above and their effect upon the final results. Section 4 outlines our approach to computing the AO sky coverage function $P(S \geq S_0)$, the probability of obtaining a Strehl ratio of at least S_0 under given observing conditions. Sample numerical results are presented in § 5, and § 6 is a brief summary of key conclusions. The Appendix contains a review of the radiometric formulae used for wavefront sensor (WFS) signal-to-noise ratio (SNR) calculations.

2. SYSTEM AND SCENARIO PARAMETERS

The range of input parameters required for AO sky coverage calculations is extensive. They include a basic description of the observing scenario, the guide star density function, the atmospheric turbulence and wind velocity profiles, the windshake-induced

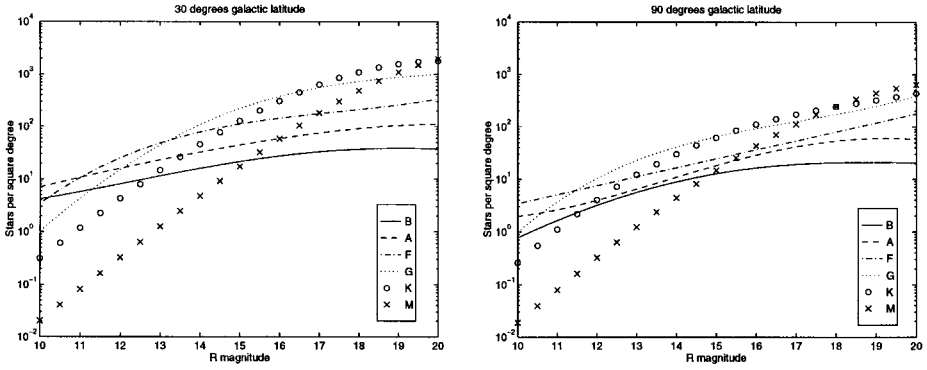

FIG. 2.—Guide star density functions

TABLE 1
RADIOMETRIC ZERO POINTS FOR TIP/TILT SENSING BY GUIDE STAR SPECTRAL CLASS

Spectral Class	Zero Point[a] (photons m^{-2} s^{-1})
B	8.71×10^{9}
A	1.57×10^{10}
F	2.41×10^{10}
G	3.05×10^{10}
K	5.74×10^{10}
M	1.72×10^{11}

[a] $J+H$ band.

tip/tilt jitter spectra, the overall AO system architecture, and parameters for AO system components including the WFSs, the deformable mirror (DM), and the control algorithm. The values assumed for these quantities are summarized in the following subsections, beginning with an overview of the basic NGS and LGS AO system architectures. A final subsection highlights some of the factors neglected in the analysis.

2.1. AO System Architectures

The NGS and LGS AO system models both include a low-order IR WFS for tip/tilt sensing and a visible WFS for higher order wavefront measurements. Outputs from the two sensors are used to drive a fast steering mirror (FSM) and a DM to correct these two classes of error using independently optimized control algorithms. The labels "NGS" and "LGS" apply only to the guide star used for higher order wavefront sensing, since both systems require a natural guide star to measure tip and tilt. The science field to be compensated is almost always displaced from the natural guide star, so both the tip/tilt and higher order corrections applied by the NGS AO system are degraded by conventional, or angular, anisoplanatism. The LGS AO system projects the laser guide star in the direction of the science field, so that only the tip/tilt correction is degraded by conventional anisoplanatism. The higher order compensation provided by the LGS AO system is degraded by focus anisoplanatism owing to the finite altitude of the laser guide star, in this case 92.5 km in the mesospheric sodium layer. The extent of the science field is assumed to be small enough so that any variability in AO performance within the field may be neglected.

All remaining parameters and design approaches for the NGS and LGS AO systems are held common except for the choice of the higher order wavefront sensing beacon. Common parameters are maintained because the LGS AO system is viewed as a planned upgrade to a NGS AO system already in the detailed design phase (Rigaut, Ellerbroek, & Northcott 1997).

An important feature of the Gemini AO system design is the placement of the DM in a plane optically conjugate to a range of 6.5 km, the mean altitude of atmospheric turbulence at the Gemini-North site. Turbulence in this plane is properly corrected by the DM for a wavefront propagating from any direction, and analysis indicates that the diameter of the field compensated by the AO system is increased by a factor of 2 or greater using this approach (Racine & Ellerbroek 1995). This yields a corresponding increase in the allowable offset between the natural guide star and the science field and significantly improves sky coverage for both the NGS and LGS AO systems. The entrance pupils of both WFSs are also placed optically conjugate to the 6.5 km altitude so that the registration between the DM and the WFSs will be independent of the direction of the guide star. As illustrated in Figure 1, this approach implies that the beam prints for the NGS, LGS, and science field are no longer coincident on the DM. For the NGS AO system, the science field beam print is translated from the NGS beam print, and no direct turbulence measurements are available to compensate the disjoint portion of the beam. In this analysis an aperture stop in a plane conjugate to the DM vignettes the unsensed region of the science field beam print.

For the LGS AO system, the diameter of the LGS beam print on the DM is only about 93% of the science field beam print, and some DM actuators at the edge of the pupil must be "slaved" because they do not couple into the LGS wavefront sensor

TABLE 2
ATMOSPHERIC TURBULENCE STATISTICS AT MAUNA KEA

Profile(s) Selected	Number of Profiles	r_0[a] (m)	θ_0 for $z = 0.0$ km[a] (arcsec)	θ_0 for $z = 6.5$ km[a] (arcsec)
0.20 m $\leq r_0 \leq$ 0.25 m	98	0.223 ± 0.014	2.38 ± 0.73	4.54 ± 1.96
GAR11N.M01 No. 8[b]	1	0.235	2.04	4.69
0.40 m $\leq r_0$	33	0.466 ± 0.075	3.52 ± 6.95	7.76 ± 2.23
DEL12N.M02 No. 3[b]	1	0.420	3.02	7.90

[a] At $\lambda = 0.5$ μm and $\psi = 0°$.
[b] Representative profile used for sky coverage calculations

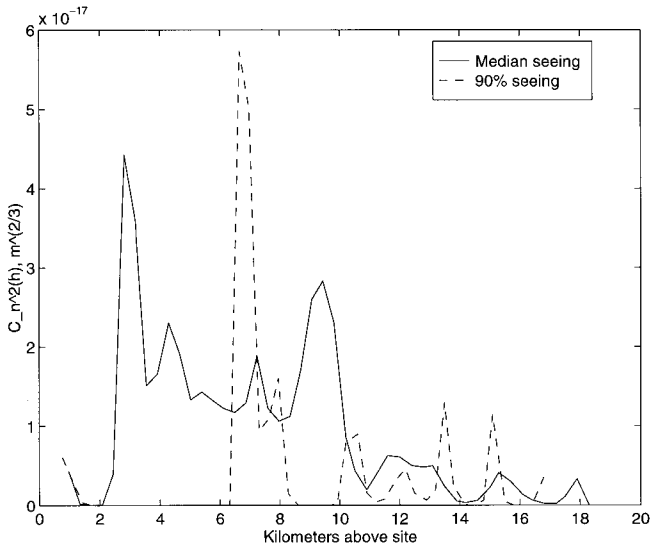

FIG. 3.—Representative Mauna Kea $C_n^2(h)$ profiles used for sky coverage calculations

measurements. The pupil of the tip/tilt WFS is also stopped down to this diameter so that any unsensed errors in the displacements of slaved actuators do not degrade the tip/tilt measurement.

The aperture stop geometries illustrated in Figure 1 have been included in the calculations for WFS SNR and the effects of anisoplanatism. Using a nonzero AO conjugate range without including such stops is theoretically possible if DM actuators can be commanded absolutely without position feedback from the WFS. Sample results in Racine & Ellerbroek (1995) for the NGS AO case indicate that eliminating the aperture stop degrades the Strehl ratio with an off-axis guide star owing to the larger wavefront estimation errors in the unsensed part of the beam. The absolute on-axis intensity of the image of a point source will, however, improve by about 5%–10% owing to the increased area of the collecting aperture.

2.2. Observing Scenarios, Guide Stars, and Sky Backgrounds

The Gemini "8 m" telescope aperture diameter is $D = 7.9$ m, with a linear central obscuration ratio of 0.152. AO system performance has been evaluated for wavelengths of 1.25, 1.65, and 2.2 μm (J, H, and K bands), at telescope zenith angles of 0° and 45°.

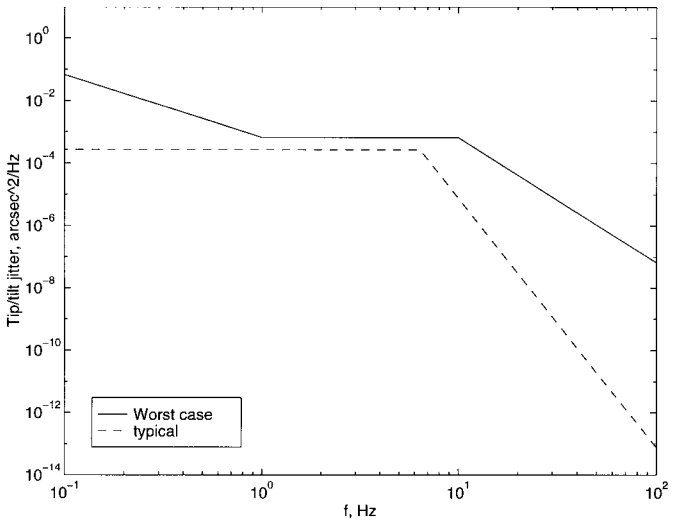

FIG. 4.—Typical and worst case windshake-induced tip/tilt jitter spectra

TABLE 3
FIRST-ORDER AO SYSTEM PARAMETERS

Parameter	NGS HO	LGS HO	Tip-Tilt
WFS subapertures	12 × 12	12 × 12	2 × 2
Sensing band	0.4–0.8 μm	0.589 μm	$J+H$
Radiometric zero point (photons m^{-2} s^{-1})	4.38×10^{10}	[a]	See Table 1
Atmospheric attenuation (mag air $mass^{-1}$)	0.150	0.150	0.050
Optics + detector efficiency	0.344	0.344	0.344
Noise electrons per pixel per read	3	3	8
Sky background (photons m^{-2} s^{-1} $arcsec^{-2}$)	332	0	6890
Pixel subtense (arcsec)	0.250	0.250	0.170
DM actuators	13 × 13	13 × 13	NA
Sampling rate (Hz)	10–1000, adjustable[b]		
Control bandwidth (Hz)	(sampling rate)/10		
Loop dynamics	Pure integrator		

[a] 2×10^5 photons m^{-2} s^{-1} W^{-1} at telescope aperture.
[b] Independently adjustable for tilt and higher order compensation.

Guide star density functions have been derived by Doug Simons using the Bahcall-Soneira model (Bahcall & Soneira 1980). Guide star densities are parameterized by the function $\rho(R)$, the expected number of guide stars per square degree with R-band magnitude no dimmer than R. Separate density functions have been computed for class B, A, F, G, K, and M stars because the NGS AO system incorporates wavefront sensors operating in two different spectral bands. Density functions corresponding to 30° and 90° Galactic latitude have been computed for each spectral class. These specific latitudes are not entirely consistent with zenith angles of 0° and 45° at the Gemini-North site, so it is best to view these functions more generically as "dense" and "sparse" cases. The guide star density functions are plotted in Figure 2. G and K are the most common spectral classes for stars with magnitudes between 14 and 17. This is about the limiting magnitude for diffraction-limited atmospheric turbulence compensation using NGS AO for Gemini (Rigaut et al. 1997).

Guide star signal levels and sky background levels are required inputs for evaluating WFS tilt measurement accuracy and its effect on AO system performance. As specified to us by the Gemini project, the zero point for higher order WFS radiometry calculations is defined as the photon flux from a 0 mag K star in the 0.4–0.8 μm passband at the top of the atmosphere. This yields a numerical value of 4.38×10^{10} photons m^{-2} s^{-1}. The passband is broader than the R band, and variations of up to 22% (0.22 mag) in signal level depending upon the spectral class of the guide star have been neglected. Since guide star brightness is parameterized by R magnitude, these variations are much more significant in the IR ($J+H$) passband used for tip/tilt sensing by both the NGS and LGS AO systems. Table 1 lists the zero point for this passband as a function of guide star spectral class. For the LGS AO system, the analog of a zero point is the signal level obtained with a 1 W beacon laser. Recent experiments report

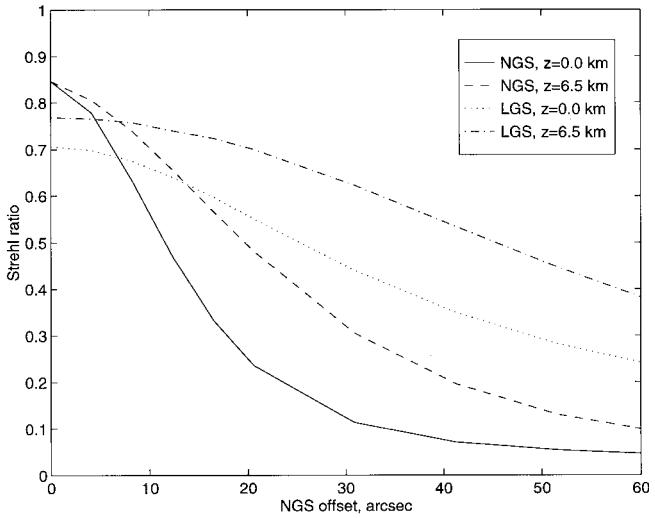

FIG. 5.—Strehl reduction due to NGS offset for NGS and LGS AO systems and AO conjugate ranges (z) of 0.0 and 6.5 km

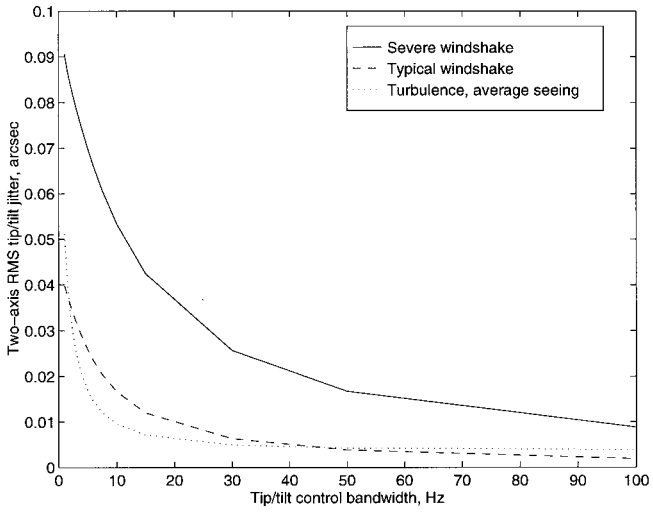

FIG. 6.—Residual tip/tilt jitter vs. control bandwidth for windshake and atmospheric turbulence

a value of 2×10^5 photons m^{-2} s^{-1} W^{-1} including the two-way atmospheric transmittance loss at zenith for a pulsed, Nd:Yag-pumped dye laser developed at Lawrence Livermore National Laboratory (Avicola et al. 1994). Considerably different values for the zero point might be obtained with other beacon laser designs. The laser powers considered here are low enough to neglect saturation effects. Also, the angular subtense of the laser guide star has been computed as described in the Appendix assuming a 0.5 m diameter launch telescope located behind the Gemini secondary mirror.

Values for the sky background have been provided to us by the Gemini project. The moonless sky background on Mauna Kea in the *R* band is 20.3 mag $arcsec^{-2}$, which corresponds to 332 photons m^{-2} s^{-1} $arcsec^{-2}$ at the top of the atmosphere with the zero point we have assumed for the visible wavefront sensor passband of 0.4–0.8 μm. This approximate value is negligible compared with the expected detector read noise and the signal levels necessary for higher order wavefront sensing. For the *J*+*H* tip/tilt sensing band the background is 6.890×10^3 photons m^{-2} s^{-1} $arcsec^{-2}$, which can be more significant.

2.3. Atmospheric Profiles and Windshake

Median and 90th percentile seeing conditions reported at the Gemini-North site on Mauna Kea correspond to r_0 values of 0.24

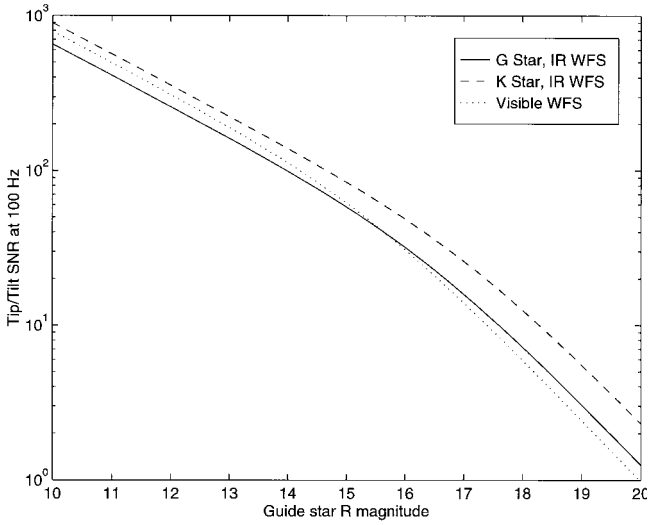

FIG. 7.—Effective tip/tilt sensor SNR vs. guide star *R* magnitude for IR and visible wavelength tip/tilt sensing

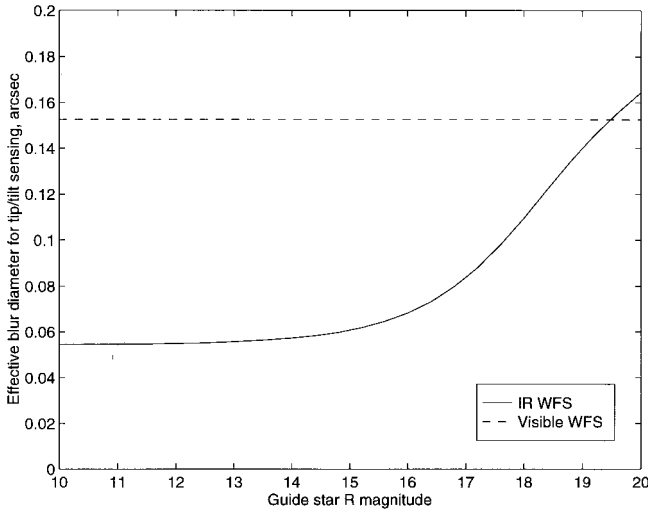

FIG. 8.—Effective guide star blur diameters for IR and visible wavelength tip/tilt sensing with NGS higher order wavefront sensing

and 0.42 m at a wavelength of 0.5 μm (Racine et al. 1991). AO system sky coverage also depends strongly upon the isoplanatic angle θ_0, and information on the vertical distribution of atmospheric turbulence is required for these calculations. Such data were collected by F. Roddier during 1987–1988 using the scidar technique (Roddier 1992). Table 2 lists statistics on the distribution of θ_0 for subsets of the measured profiles with r_0 values corresponding approximately to either median or 90th percentile seeing. Changing the AO conjugate range from 0.0 to 6.5 km increases θ_0 by about a factor of 2 in both cases. The two specific $C_n^2(h)$ turbulence structure profiles used for these sky coverage calculations are plotted in Figure 3, and Table 2 lists the associated values of r_0 and θ_0. The value of r_0 scales as $\lambda^{6/5} \cos^{3/5} \psi$, where ψ is the zenith angle. The value of θ_0 scales as $\lambda^{6/5} \cos^{8/5} \psi$ if the AO conjugate *altitude* is held constant. Since the Gemini system employs a fixed AO conjugate *range* of 6.5 km to simplify the AO system optical design, θ_0 actually degrades more rapidly with increasing zenith angle. Providing a scaling law for θ_0 as a function of ψ is not possible in this case because the degradation will vary depending upon the shape of the $C_n^2(h)$ profile.

The mean surface wind velocity at CFHT on Mauna Kea is 13 knots (6.7 m s^{-1}), and the mean maximum wind velocity in the troposphere is 52 knots (26.8 m s^{-1}) at an altitude of 7.8 km above Mauna Kea (Bely 1987). Based upon these two points, we have assumed a wind velocity profile $v(h) = 13 + 39(h/7.8)$ knots for $0 \leq h \leq 7.8$ km, and $v(h) \equiv 52$ knots for $h \geq 7.8$ km above the Mauna Kea site. This profile yields a Greenwood frequency, f_G, of 39.25 (26.97) Hz for $\lambda = 0.5$ μm, $\psi = 0°$, and the median

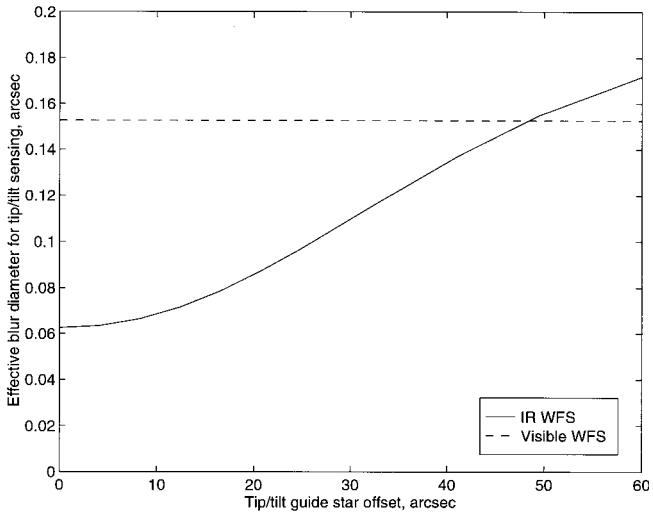

FIG. 9.—Effective guide star blur diameters for IR and visible wavelength tip/tilt sensing with LGS higher order wavefront sensing

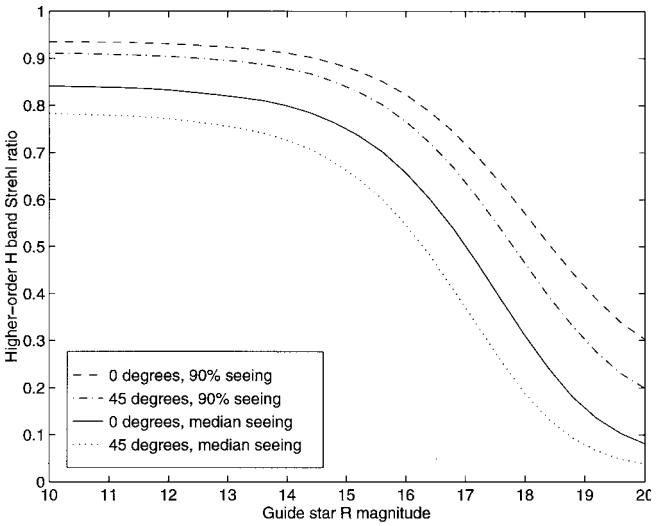

FIG. 10.—Optimized higher order *H*-band Strehl ratios with an on-axis NGS vs. guide star magnitude, seeing, and zenith angle

(90th percentile) $C_n^2(h)$ profiles plotted in Figure 3. The value of f_G scales as $\lambda^{-6/5}$. The zenith angle scaling of f_G depends upon the direction of the wind relative to the zenith angle. The worst case scaling of $\cos^{-3/5}\psi$ occurs when these two directions are orthogonal and has been used in this analysis.

The surface wind blowing on the telescope and its enclosure induces "windshake," which can be a significant source of tip/tilt jitter requiring compensation by the AO system. Figure 4 plots the two windshake-induced tip/tilt jitter power spectral densities (PSDs) used in this study. These piecewise linear functions are fits to more detailed NASTRAN modeling performed by the Gemini project (R. McGonegal 1996, private communication). Both PSDs correspond to a ground wind speed of 8.4 m s^{-1}. For the "worst case" power spectrum, the telescope is pointing into the wind at a 60° zenith angle. The "typical" spectrum was computed for a 45° zenith angle with the wind blowing from the side. The integrals of these two PSDs yield rms image motion jitter values of 0″.137 and 0″.037. Results presented in § 3 below indicate that this source of image motion can be more difficult to compensate than turbulence-induced tip/tilt.

2.4. AO System Components and Parameters

Components of both the NGS and LGS AO system include a visible wavelength Shack-Hartmann WFS for higher order sensing, an IR Shack-Hartmann WFS for tip/tilt sensing, a matrix multiply wavefront reconstructor to compute the higher order wavefront

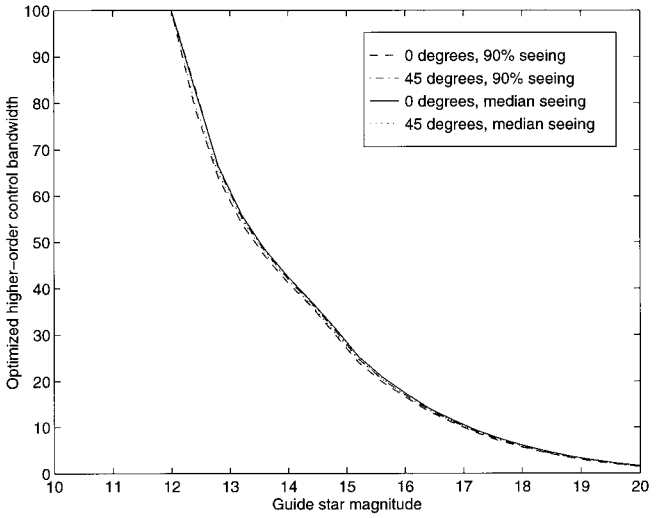

FIG. 11.—Optimal higher order control bandwidth vs. guide star magnitude for NGS AO

TABLE 4
WFS SIGNAL LEVELS FOR LGS AO PERFORMANCE ANALYSIS[a]

Sampling Rate (Hz)	ψ(deg)	Signal Level[b]	SNR
1000	0	448	20.4
	45	283	15.8
500	0	896	29.3
	45	565	23.1

[a] LGS intensity of 0.3 photons cm^{-2} ms^{-1} at the telescope aperture at zenith.
[b] Photodetection events per subaperture per frame.

correction, servo loop compensation to filter the higher order and tip/tilt error estimates temporally, and a DM and fast steering mirror (FSM) to apply the wavefront correction. The basic parameters for these components are listed in Table 3, with further details on modeling assumptions given in the following paragraphs.

The two Shack-Hartmann WFSs used for higher order and tip/tilt wavefront sensing contain 12 × 12 and 2 × 2 subapertures, respectively. Subaperture tilt measurements are modeled as the sum of the average wavefront gradient within the subaperture and normally distributed noise. The magnitude of the noise is computed using a quadrant detector model as described in the Appendix (Tyler & Fried 1982; Welsh et al. 1995). For the large subapertures found in the IR tip/tilt WFS, the partial "sharpening" of the guide star images by the higher order adaptive optics significantly improves tip/tilt measurement accuracy and has been included in the analysis. Measurements from partially illuminated subapertures at the edge of the telescope have their rms noise levels increased accordingly.

The continuous facesheet DM has 13 × 13 actuators located optically conjugate to the corners of the subapertures in the higher order WFS. The DM wavefront correction is modeled assuming linear superposition of the commands to the individual actuators, with a uniform actuator influence function given by a linear spline of the form

$$p_i(x, y) = \begin{cases} \left[1 - \left(\frac{|x - x_i|}{w}\right)\right]\left[1 - \left(\frac{|y - y_i|}{w}\right)\right], & \max\left(|x - x_i|,\ |y - y_i|\right) \le w, \\ 0, & \text{otherwise}, \end{cases} \tag{2.1}$$

where (x_i, y_i) is the location of actuator number i and w is the interactuator spacing. The coupling of edge DM actuators into WFS measurements accounts for the partial illumination of the edge subapertures.

The tip/tilt control loop computes its error signal as an arithmetic average of the tip/tilt measurements from the four subaperture IR WFS. The higher order control loop employs a matrix multiply wavefront reconstructor with coefficients optimized as a function of the WFS noise level, the guide star location, and the atmospheric turbulence $C_n^2(h)$ profile to minimize the residual mean-square wavefront error in the direction of the science field (Ellerbroek 1994). Constraints are imposed to guarantee the stability of the AO control loop. The reconstructor is "modal" in the sense that a higher order mode will be left uncontrolled if the expected estimation error due to noise and anisoplanatism becomes larger than the open-loop error, but all modes that are corrected are compensated at a single, globally optimized bandwidth. This approach is simpler to evaluate than full modal control with independently optimized bandwidths for each wavefront mode, and the associated performance penalty is negligible in comparison with other error sources (Ellerbroek et al. 1994).

The control bandwidths for the higher order and tip/tilt control loops are optimized independently to minimize the combined effect of noise and servo lag for the associated WFS parameters and input disturbance. The servo control law is a pure integrator with a closed-loop impulse response function given by the equation $f(t) = 2\pi f_{3db} \exp(-2\pi f_{3db} t)$, where f_{3db} is the control bandwidth. The WFS sampling rate is fixed at 10 times the control bandwidth, and the effects of signal processing latency and the temporal dynamics of the DM and FSM upon the impulse response function have been neglected. The control bandwidths and the wavefront reconstruction algorithm are optimized assuming a priori knowledge of the $C_n^2(h)$ and windspeed profiles, but not the wind direction.

TABLE 5
HIGHER ORDER STREHL RATIOS FOR LGS AO

ψ(deg)	Seeing	J	H	K
0	Median	0.640	0.774	0.865
	90%	0.841	0.905	0.945
45	Median	0.520	0.685	0.807
	90%	0.775	0.863	0.920

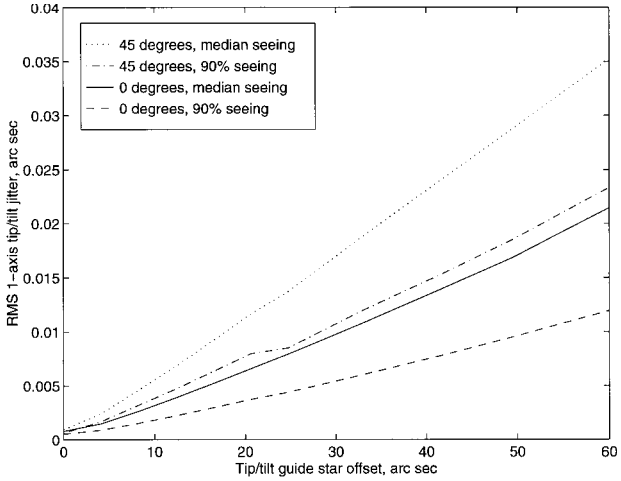

FIG. 12.—Anisoplanatic tip/tilt jitter vs. guide star offset with NGS AO

AO system performance estimates are therefore average values derived assuming a uniform distribution for the direction of the wind.

2.5. Neglected Factors and Simplifications

The range of inputs required by these sky coverage calculations is so large that a full exploration of the parameter space is clearly impractical. This is particularly true for the guide star density function, the telescope zenith angle, and the atmospheric $C_n^2(h)$ and windspeed profiles. The subset of scenarios considered here spans some of the bounds of this space and indicates the comparative performance of the NGS and LGS AO systems for a range of typical test cases.

All of the Strehl ratio values presented in this paper apply to the AO system alone, since the effect of fixed optical aberrations in the telescope and science instrument has been neglected. Incorporating these errors to obtain overall performance estimates for Gemini is nontrivial, since the shape of the overall point-spread function (PSF) and its relationship to the instrument's slit width or pixel size may greatly influence the SNR or angular resolution associated with a given Strehl ratio (Tyler & Ellerbroek 1998). Sky coverage calculations are further complicated if the fixed optical aberrations are field-angle dependent. Useful estimates of the end-to-end system PSF can usually be obtained by convolving separately computed transfer functions for the AO system and

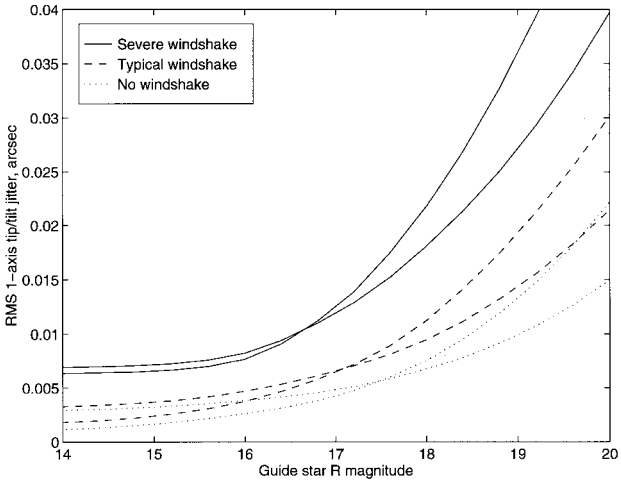

FIG. 13.—Tip/tilt jitter due to noise and servo lag for an on-axis guide star. For each windshake condition the higher (lower) curve at the right corresponds to a NGS (LGS) AO system. These results are for median seeing, a zenith angle of 0°, and a K-class guide star.

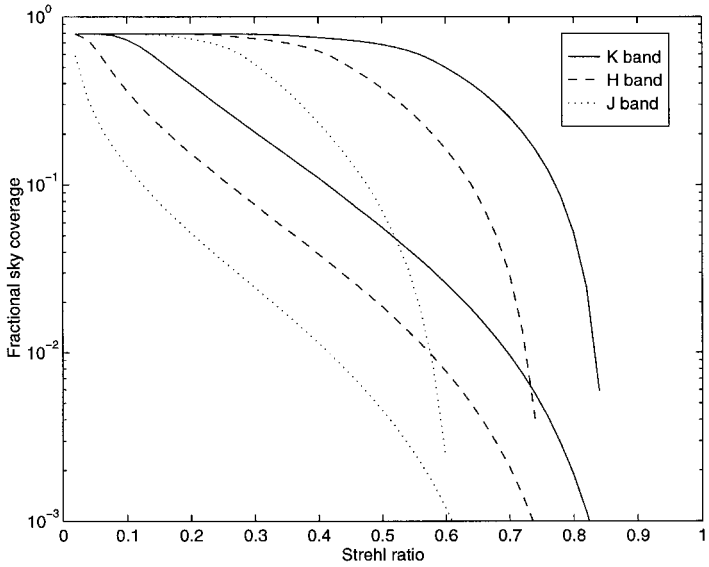

FIG. 14.—Nominal sky coverage probabilities at 90° Galactic latitude. For each spectral band the lower (higher) curve corresponds to the NGS (LGS) AO system. These results are for the case of median seeing, a zenith angle of 0°, and typical windshake.

the telescope/instrument combination, but the latter function depends upon the instrument and the observing band and is not fully characterized at the time of this writing.

Various parameters for the Gemini AO system are not yet fully defined and have been approximated in the interests of timeliness. The pure integrator control laws assumed for the higher order and tip/tilt control loops neglect the latencies associated with signal processing and WFS integration time, which may be significant when long integration times are required for dim guide stars. The temporal dynamics of the DM and FSM have not been considered, and the latter may become significant if a high tip/tilt control bandwidth is required to compensate strong windshake. It will probably not be possible to optimize the AO control algorithm fully based upon a priori knowledge of atmospheric parameters and the guide star signal level, but recent simulations indicate that

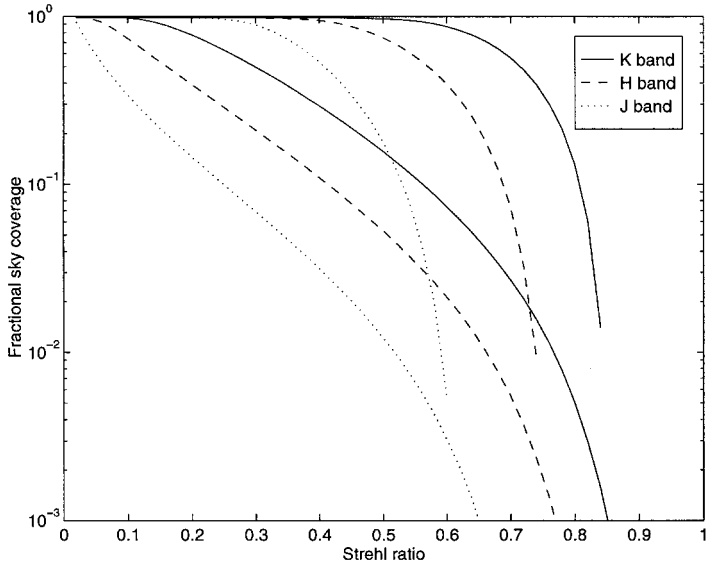

FIG. 15.—Nominal sky coverage probabilities at 30° Galactic latitude. For each spectral band the lower (higher) curve corresponds to the NGS (LGS) AO system. These results are for the case of median seeing, a zenith angle of 0°, and typical windshake.

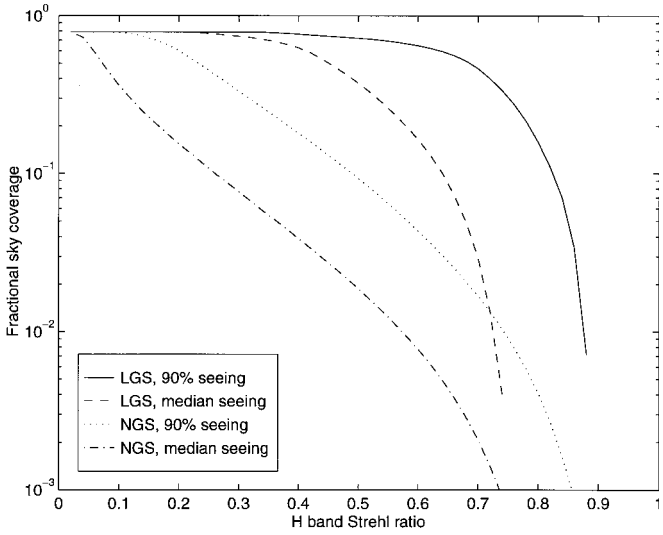

FIG. 16.—Impact of seeing upon sky coverage. These results are for a Galactic latitude of 90°, a zenith angle of 0°, and typical windshake.

almost equivalent levels of performance can be achieved with a fixed reconstructor as long as the AO control loop bandwidth can be adjusted in real time (Rigaut et al. 1997). Detector read noise has been treated as independent of detector read rate, and a rms read noise value of 3 electrons per pixel per read has not yet been demonstrated for frame rates higher than about 300 Hz. We do not expect that any of the above approximations will have much of an effect upon sky coverage estimates for high Strehl ratios above about 0.4 with typical windshake conditions, since this level of performance requires a relatively bright guide star for which the effects of detector read noise and WFS integration time are secondary. For tip/tilt compensation, all of the factors should affect the NGS and LGS sky coverage estimates equally because the analysis for both systems is based upon common WFS parameters, servo loop compensation, and guide star density models. For higher order correction, the LGS AO system is less sensitive to the values chosen for WFS latency and detector read noise because the laser guide star provides high signal levels at a high sampling rate.

The WFS pupil and aperture stop geometry illustrated in Figure 1 is not entirely correct for the Gemini-North system because the entrance pupil for the 2 × 2 subaperture tip/tilt WFS is fixed in a plane optically conjugate to the primary mirror to eliminate the need for a cryogenic moving part. The actual Gemini configuration will increase tilt anisoplanatism somewhat because the

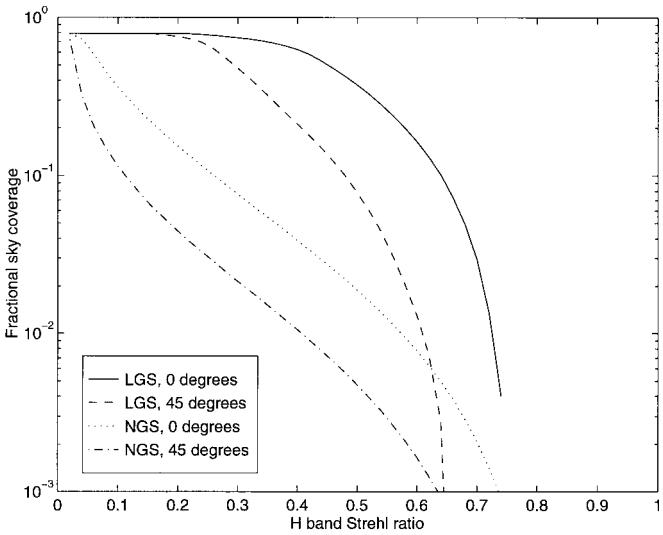

FIG. 17.—Impact of zenith angle upon sky coverage. These results are for a Galactic latitude of 90°, median seeing, and typical windshake.

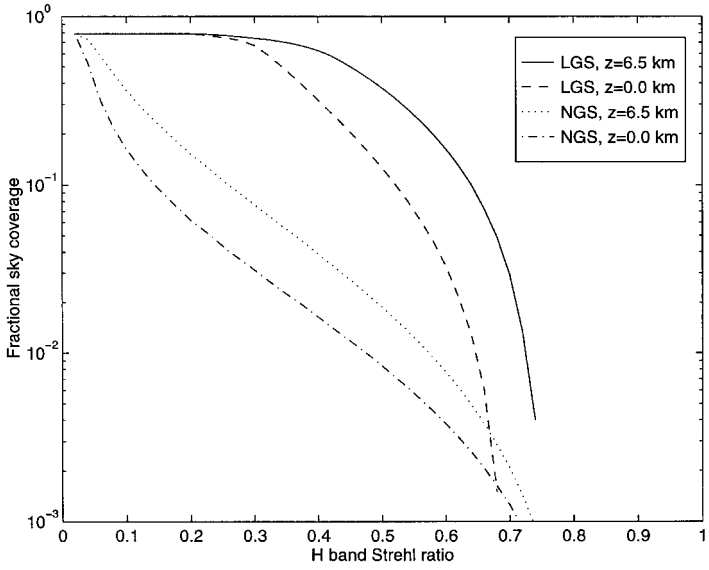

FIG. 18.—Impact of AO conjugate altitude upon sky coverage. These results are for a Galactic latitude of 90°, a zenith angle of 0°, median seeing, and typical windshake.

tracking beam print at $z = 6.5$ km is sheared outside of the region sensed and compensated by the higher order WFS. The quantitative magnitude of this tilt error depends upon the accuracy with which the higher order wavefront measurement can be extrapolated into this region, and we are unable to evaluate this effect because the current version of our analysis code requires that all WFSs be placed conjugate to a single plane. "Slaved" DM actuators outside of the WFS beam print that are driven open-loop will also introduce small tilt errors if they are not commanded precisely.

For both AO systems, it is possible that improved higher order wavefront estimates could be obtained by augmenting the higher order WFS measurements with measurements from the 2×2 subaperture tip/tilt WFS. For the NGS AO system, combining the output of both sensors could conceivably improve tip/tilt sensing accuracy as well. Evaluating any improvement in sky coverage associated with these approaches is difficult because the SNRs for the two wavefront sensors vary separately as a function of guide star magnitude and spectral class. This level of sophistication will be left for later.

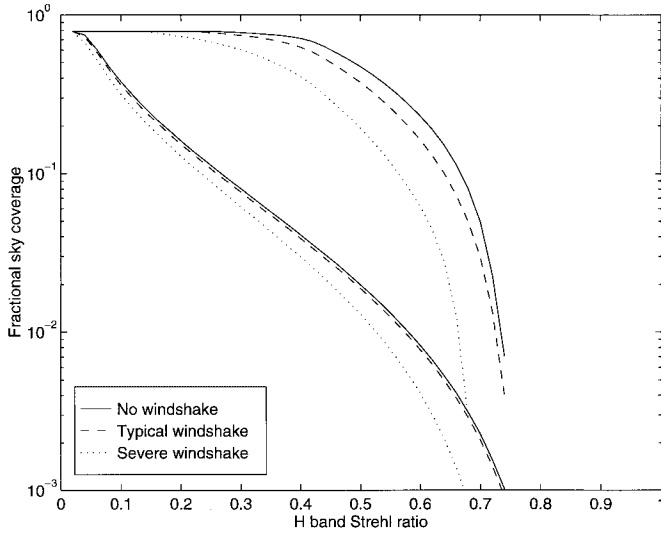

FIG. 19.—Impact of windshake upon sky coverage. For each windshake model, the lower (higher) curve corresponds to the NGS (LGS) AO system. These results are for a Galactic latitude of 90°, a zenith angle of 0°, and median seeing.

3. PERFORMANCE DRIVERS

The choice of NGS or LGS wavefront sensing is only one of several design options that have significant impacts on the sky coverage achieved by the AO system. Three others are the choice of the AO conjugate altitude, the values assumed for windshake-induced tip/tilt jitter, and the use of a separate 2 × 2 subaperture IR wavefront sensor for tip/tilt sensing. Sample results highlighting the importance of these effects are described in the following subsections. Following this intermission, §§ 4 and 5 below continue with a systematic development of the sky coverage analysis.

3.1. AO Conjugate Altitude

As mentioned previously, the DM and the entrance pupils for both WFSs comprising the Gemini-North AO system are located in planes optically conjugate to a range of 6.5 km. This range corresponds to the mean altitude of turbulence at the telescope site, and the isoplanatic angles computed for measured Mauna Kea $C_n^2(h)$ profiles are approximately doubled using this configuration. Figure 5 describes the associated increase in the *H*-band Strehl ratio with an off-axis natural guide star for the case of median seeing and a zenith angle, ψ, of 0°. WFS noise, servo lag, and telescope windshake are neglected for these calculations, so the only error sources contributing to these Strehl ratios are anisoplanatism and DM/WFS fitting error. The horizontal axis gives the offset between the natural guide star and the science field. This star is used for both tip/tilt and higher order wavefront sensing by the NGS AO system, while the LGS AO system measures the higher order wavefront using a laser beacon projected toward the science field at a range of 92.5 km in the mesospheric sodium layer. The vertical axis plots long-exposure Strehl ratios for NGS and LGS AO systems with AO conjugate ranges of either 0.0 or 6.5 km.

Figure 5 indicates that an AO conjugate altitude of 6.5 km approximately doubles the allowable offset to the natural guide star for an *H*-band Strehl ratio in the 0.5–0.6 range. This result is obtained with either NGS or LGS higher order wavefront sensing. In addition to the effect of AO conjugate altitude, Figure 5 also illustrates the relative performance of NGS and LGS AO with an off-axis natural guide star. The on-axis, or zero-offset, performance of the NGS AO system is superior because it is not degraded by focus anisoplanatism. The performance of the LGS AO system becomes superior for natural guide star offsets greater than about 10″ because the natural guide star is used only for tip/tilt compensation and not for higher order correction. The allowable natural guide star offset for an *H*-band Strehl ratio in the 0.5–0.6 range is approximately doubled using LGS AO for either choice of AO conjugate altitude. These LGS AO Strehl ratios apply at the center of the science field in the direction of the laser beacon used for higher order wavefront sensing. The performance variations about this point will be very similar to those for an NGS AO system with an on-axis guide star.

3.2. Windshake

Tip/tilt jitter induced by windshake can place severe requirements on the bandwidth of the AO system, more so than atmospheric turbulence itself. Figure 6 plots residual rms tip/tilt jitter as a function of tip/tilt control bandwidth for the two windshake PSDs plotted in Figure 4 and for turbulence-induced tip/tilt with median seeing. The residual errors for typical windshake and atmospheric turbulence are roughly comparable, but the errors for severe windshake are greater by a factor of 3–4 for control bandwidths in the range from 10 to 100 Hz. Severe windshake increases the control bandwidth necessary for a given level of tip/tilt compensation by a similar factor, thereby increasing the required signal level for the tip/tilt guide star and significantly reducing sky coverage. These considerations are quantified in the numerical sky coverage results presented in § 5.

3.3. IR Tip/Tilt Sensing

The IR instruments planned for the Gemini-North telescope will incorporate "on-instrument wavefront sensors" with 2 × 2 subapertures to measure tip/tilt and focus misalignments between the instrument and the telescope (Oschmann 1995). The NGS AO system may use either this sensor or the visible WFS with 12 × 12 subapertures for high-bandwidth tip/tilt compensation. The IR wavefront sensor provides equal or better performance for all cases of interest, due to both SNR considerations and the compensation (or "sharpening") of the guide star images in the tip/tilt sensor subapertures by the higher order adaptive optics.

For the case of quadrant detector tilt sensing using 4 active pixels per subaperture, the one-axis, 1 σ subaperture tilt measurement error for either WFS can be described by the formula

$$\sigma_\theta = \frac{\theta_B}{\mathrm{SNR}}, \tag{3.1}$$

where σ_θ is the rms tip/tilt error, θ_B is the effective diameter of the guide star image in a single WFS subaperture, and SNR is the signal-to-noise ratio summed over the 4 active pixels (Tyler & Fried 1982; Welsh et al. 1995). For a full aperture tip/tilt measurement

computed as the average measurement from a WFS with N subapertures, this rms tilt error may be divided by $\sqrt{N}$, or equivalently the SNR term in this expression may be replaced by the total signal-to-noise ratio summed over all the active pixels in all subapertures. For the radiometric parameters listed in Table 3 above, the 2 × 2 subaperture IR WFS is generally superior to the 12 × 12 subaperture visible WFS in terms of both θ_B and total SNR.

Figure 7 plots SNR at a representative 100 Hz sampling rate versus the R magnitude of the guide star for the two WFS options and G- and K-class guide stars, the two most common spectral classes at intermediate magnitudes. For K stars, the IR WFS SNR is always superior because of the relative signal levels in the two sensor passbands. For G stars, the visible WFS SNR is superior for bright guide stars because the signal level is greater in the visible passband, but it degrades more rapidly for dim guide stars because of the greater level of detector noise associated with the larger number of subapertures in the visible WFS. Similar results are obtained for all WFS sampling rates in the 10–1000 Hz range.

The guide star blur diameter θ_B depends upon seeing, the passband used for tip/tilt sensing, the size of the subapertures in the tip/tilt WFS, and the degree of wavefront compensation achieved within each of these subapertures by the higher order adaptive optics. Figure 8 plots the value of θ_B for IR and visible tip/tilt sensing as a function of guide star R magnitude. These results are for the case of higher order NGS AO, median seeing, and a zenith angle of 0°. The value of θ_B is constant for the visible WFS because there is no higher order correction within the individual subapertures. θ_B varies with magnitude for the IR WFS because the degree of correction achieved within each of these larger subapertures depends upon the SNR for the higher order, visible WFS. The blur diameter is significantly smaller for the IR WFS for all but the dimmest guide stars because (1) the diffraction-limited blur diameter is smaller, (2) the effect of seeing is more benign at the longer wavelength, and (3) the degree of higher order compensation achieved by the NGS AO system is quite good in the direction of the guide star. Combining the results in Figures 7 and 8 according to equation (3.1) indicates that the IR WFS will provide better tip/tilt sensing accuracy over the entire range of possible magnitudes for the most common guide star spectral classes.

The images of the tip/tilt guide star in the IR WFS are also sharpened by higher order adaptive optics for the case of LGS AO. The degree of sharpening no longer depends upon the magnitude of the tip/tilt guide star, since the higher order wavefront measurement is obtained using an independent laser guide star with a fixed (and fairly high) SNR. The degree of compensation will, however, be degraded by anisoplanatism because the laser beacon is projected in the direction of the science field, which is usually not the direction of the tip/tilt guide star. Figure 9 plots the effective blur diameter θ_B as a function of the offset between these two directions, with the blur diameter for the visible 12 × 12 subaperture WFS plotted for comparison. The effect of anisoplanatism becomes significant for guide star offsets larger than about 20″, but the IR WFS blur diameter remains smaller than the visible WFS blur diameter for separations of up to 45″, which is 75% of the radius of the Gemini AO guide field.

4. ANALYSIS APPROACH

AO system sky coverage is parameterized below in terms of the function $P(S \geq S_0)$, the probability of achieving a Strehl ratio at least equal to some threshold S_0. This probability may be treated as a deterministic fraction when sky coverage is averaged over a nonnegligible fraction of the sky. The function $P(S \geq S_0)$ is implicitly a function of the observing scenario, the guide star density profile, atmospheric conditions, windshake, and AO system parameters. To derive a formula for this function, let $N(S_0)$ be the number of guide stars that are sufficiently bright and close enough to the science field to provide a Strehl ratio of at least S_0. Treating the distribution of guide stars as a Poisson process, the value of $P(S \geq S_0)$ is given by

$$\begin{aligned} P(S \geq S_0) &= P[N(S_0) \geq 1] \\ &= 1 - \exp\,[-\bar{N}(S_0)], \end{aligned} \tag{4.1}$$

where $\bar{N}(S_0)$ is the expected value of $N(S_0)$ averaged over the ensemble of science fields.

Computing the function $N(S_0)$ requires knowledge of the guide star density function, as well as a model for AO system performance as a function of guide star magnitude and spectral class. Let $\rho_c(R)$ be the density of guide stars of spectral class $c \in C =$ {B, A, F, G, K, M} with R-band magnitude no dimmer than R, and let $\theta(S_0, R, c)$ be the maximum allowable offset from the science field to achieve a Strehl ratio of at least S_0 with a guide star of this magnitude and spectral class. The function $\theta(S_0, R, c)$ is implicitly a function of the same scenario and AO system parameters as listed above for $P(S \geq S_0)$. The area of the allowable guide field to obtain a Strehl ratio of S_0 with a guide star of magnitude R and class c is $\pi\theta^2(S_0, R, c)$, and the expected number of class c stars in this field in the magnitude range $[R, R + dR]$ is $dR\rho_c'(R)\pi\theta^2(S_0, R, c)$. Integrating this value over the range of

guide star magnitudes and summing over spectral classes gives the result

$$\bar{N}(S_0) = \pi \sum_{c \in C} \int_0^\infty dR\, \rho_c'(R)\theta^2(S_0, R, c), \tag{4.2}$$

for the expected number of guide stars which provide a Strehl ratio of at least S_0 in the science field. Note that the domain of integration in this expression is effectively finite because the function $\theta^2(S_0, R, c)$ is identically zero for sufficiently large values of R. Substituting equation (4.2) into equation (4.1) and rearranging slightly yields

$$P(S \geq S_0) = 1 - \exp\left[- \int_0^\infty dR \sum_{c \in C} \rho_c'(R)\pi\theta^2(S_0, R, c) \right], \tag{4.3}$$

which is the formula used by this study to evaluate AO system sky coverage in terms of the functions $\rho_c(R)$ and $\theta(S_0, R, c)$.

Equation (4.3) is different from the approach used for sky coverage calculations in several previous papers (Rigaut & Gendron 1992; Olivier et al. 1993; Parenti & Sasiela 1994). In terms of the present notation, this earlier approach is equivalent to the formula

$$\Pi(S \geq S_0) = \max_{R_0} \{1 - \exp[-\rho(R_0)\pi\theta^2(S_0, R_0)]\}. \tag{4.4}$$

The guide star magnitude R_0 is chosen to maximize the fraction of the sky no further than $\theta(S_0, R_0)$ from a star no dimmer than magnitude R_0. Equation (4.4) underestimates sky coverage for even the optimized value of R_0 because it does not consider either (1) the larger offset to the science field allowed when the guide star is brighter than magnitude R_0 or (2) the nonzero contribution to sky coverage provided by guide stars with magnitudes fainter than R_0. To see this more explicitly, equation (4.4) may be rewritten in the form

$$\begin{aligned} \Pi(S \geq S_0) &= 1 - \exp\left\{ - \max_{R_0} [\rho(R_0)\pi\theta^2(S_0, R_0)] \right\} \\ &= 1 - \exp\left\{ - \max_{R_0} \left[\int_0^{R_0} dR\, \rho'(R)\pi\theta^2(S_0, R_0) \right] \right\}. \end{aligned} \tag{4.5}$$

The integrals in equations (4.5) and (4.3) (for a single spectral class) satisfy the inequality

$$\int_0^{R_0} dR\, \rho'(R)\pi\theta^2(S_0, R_0) \leq \int_0^\infty dR\, \rho'(R)\pi\theta^2(S_0, R), \tag{4.6}$$

since the integrands on both sides are nonnegative and $\theta(S_0, R)$ is a decreasing function of R. It follows that $\Pi(S \geq S_0)$ consistently underestimates $P(S \geq S_0)$, although we have not evaluated the magnitude of the difference for actual numerical calculations.

Figure 2 in § 2 above plots values for the guide star density function $\rho_c(R)$. The allowable guide star offset $\theta(S_0, R, c)$ can be computed by numerically inverting an array of values for the function $S(\theta, R, c)$, the overall AO system Strehl ratio as a function of θ, R, and c for an optimized reconstruction algorithm and choice of control bandwidths. This Strehl ratio is obtained from a point-spread function (PSF) computed as a convolution of tip/tilt and higher order contributions,

$$\mathrm{PSF}(\theta, R, c) = \begin{cases} \mathrm{PSF}_{\mathrm{ho}}(\theta, R) * \mathrm{PSF}_{\mathrm{tt}}(\theta, R, c), & \text{NGS AO}, \\ \mathrm{PSF}_{\mathrm{ho}} * \mathrm{PSF}_{\mathrm{tt}}(\theta, R, c), & \text{LGS AO}, \end{cases} \tag{4.7}$$

where $\mathrm{PSF}_{\mathrm{ho}}$ and $\mathrm{PSF}_{\mathrm{tt}}$ are the higher order and tip/tilt point spread functions, respectively. The higher order PSF is computed from the second-order statistics of the residual turbulence-induced wavefront errors for an optimal wavefront reconstruction algorithm and control bandwidth. This calculation accounts for the combined effects of noise, fitting error, anisoplanatism, and servo lag as

described previously (Ellerbroek 1994). For LGS AO, the higher order PSF does not depend upon the magnitude or offset of the natural guide star used for tip/tilt sensing.

The long-exposure tip/tilt PSF is modeled as a normal distribution with distinct standard deviations in the directions parallel and transverse to the offset of the tip/tilt guide star from the science field. In each of these axes, the standard deviation is computed as the root sum square of independent contributions due to windshake, measurement noise, and atmospheric turbulence:

$$\sigma(\theta, R, c; f) = [\sigma_w^2(f) + \sigma_n^2(\theta, R, c; f) + \sigma_a^2(\theta; f)]^{1/2}. \quad (4.8)$$

Here σ_w, σ_n, and σ_a are the rms tip/tilt jitters due to windshake, noise, and atmospheric turbulence, respectively, and f is the tip/tilt control bandwidth that is selected to balance the competing effects of noise and servo lag and minimize the rss of these three error sources. The function $\sigma_w(f)$ is plotted in Figure 6 above. This value is split evenly between the two axes of tip/tilt, effectively averaging AO system performance estimates over all possible directions of the guide star relative to the science field. The tip/tilt error due to noise is computed using the WFS noise model described in the Appendix below. The atmospheric tip/tilt error σ_a includes the combined effects of anisoplanatism, a finite servo bandwidth, and the finite spatial resolution of the tip/tilt WFS. The parallel and transverse values of σ_n and σ_a will be different for an off-axis tip/tilt guide star.

Tabulating the function $\theta(S_0, R, c)$ according to the above prescription is the crux of the AO sky coverage analysis. The numerical computation involved is nontrivial, but it can be completed in somewhat less than a day using an IBM RS6000 workstation for a given observing scenario and set of atmospheric conditions.

5. NUMERICAL RESULTS

This section summarizes some of the AO performance and sky coverage results that have been obtained using the parameters and methods described in §§ 2 and 4 above. In interpreting these results, the reader should bear in mind the caveats listed in § 2.5 above, in particular the omission of uncommon path errors and uncorrectable mirror figure errors. Subsections 5.1 and 5.2 outline intermediate results on higher order compensation and tip/tilt performance, respectively. The final results on sky coverage probabilities are presented in § 5.3. These include a full set of results for *J*-, *H*-, and *K*-band Strehl ratios for nominal operating conditions and guide star density functions corresponding to Galactic latitudes of 30° and 90°. Additional sample results for *H*-band Strehl ratios illustrate the significance of seeing, zenith angle, AO conjugate altitude, and windshake. LGS AO typically increases the probability of a 50% Strehl ratio in the *H* band by about an order of magnitude relative to NGS AO. The other parameters listed above can have nearly as significant an impact upon sky coverage.

5.1. Higher Order Correction

Figure 10 plots the on-axis, higher order *H*-band Strehl ratio of a NGS AO system as a function of guide star magnitude for several different observing scenarios. The Strehl ratio due to fitting error alone with a very bright guide star approaches asymptotically a value between 0.78 and 0.94, depending upon the values chosen for seeing and zenith angle. The effect of noise begins to degrade performance significantly at a guide star magnitude of about 15. Both of these results are consistent with earlier findings (Rigaut et al. 1997). The optimized control bandwidths corresponding to these Strehl ratios are plotted in Figure 11. The results obtained are nearly independent of seeing and zenith angle, since both Greenwood frequency and WFS measurement error vary in a correlated way as these conditions change. The optimized control bandwidths vary from 20 to 40 Hz for guide star magnitudes between 14 and 16, and the corresponding WFS sampling rates are in the range from 200 to 400 Hz.

For a LGS AO system, the signal level for the higher order WFS will be constant and relatively high. Table 4 plots WFS signal levels at representative zenith angles and sampling rates for a LGS intensity of 0.3 photons cm^{-2} ms^{-1} at the telescope aperture. This intensity corresponds to a natural guide star magnitude of about 10.25 for the Gemini WFS spectral passband and could be obtained with a 15 W illuminator laser according to recent experimental results with a Lawrence Livermore pulsed dye laser (Avicola et al. 1994). WFS signal level depends upon zenith angle because of the fixed altitude of the mesospheric sodium layer. The WFS SNRs computed for a 1000 Hz sampling rate are high enough to eliminate measurement noise effectively as an error source for the LGS AO system.

Higher order Strehl ratios in *J*, *H*, and *K* bands for the LGS AO system are listed in Table 5 for good and median seeing and zenith angles of 0° and 45°. These results assume a 100 Hz control bandwidth and the WFS SNRs listed in Table 4, so that fitting error and focus anisoplanatism are the only significant sources of wavefront error. Comparing the *H*-band Strehl ratios against the NGS AO results plotted in Figure 10 indicates that the Strehl ratio degradation due to focus anisoplanatism is about 4%–6% for a 0° zenith angle, and about 6%–10% at 45°. The larger error at 45° occurs in part because the 6.5 km AO conjugate *range* does not match the 6.5 km mean *altitude* for atmospheric turbulence, thereby increasing the magnitude of focus anisoplanatism.

5.2. Tip/Tilt Correction

The principal tip/tilt error sources for both AO systems are anisoplanatism, WFS noise, and the effects of a finite servo bandwidth. The tip/tilt error due to anisoplanatism for an NGS AO system is plotted in Figure 12 as a function of the tip/tilt guide star offset for good and median seeing and zenith angles of 0° and 45°. The full width half-maximum of the diffraction-limited *H*-band PSF for the Gemini-North telescope is about 0.″043, and one-axis rms tip/tilt jitter values of 0.″005 and 0.″01 correspond to Strehl ratios of about 0.937 and 0.790, respectively. With median seeing and a zero degree zenith angle, tip/tilt errors in this range occur for guide star offsets between 15″ and 30″. The allowable offset can increase or decrease by a factor of 2 for the different atmospheric conditions and zenith angles considered, which indicates that sky coverage results will be strongly influenced by these parameters. The corresponding results for the LGS AO system are very similar, but variations of up to about 10% are present owing to differences in the tracker aperture geometry illustrated in Figure 1.

Figure 13 plots the rms tip/tilt jitter due to noise and servo lag for an on-axis class K guide star with median seeing and a zenith angle of 0°. The results are plotted as a function of the *R* magnitude of the guide star for NGS and LGS AO systems with severe, typical, and no windshake. For severe windshake, the residual tip/tilt jitter is significant with even the brightest guide stars because the maximum tip/tilt control bandwidth of 100 Hz is not high enough to correct the disturbance adequately. The combined effect of noise and servo lag with severe windshake exceeds 0.″01 for a guide star *R* magnitude of about 16.5, a value that significantly limits sky coverage. For typical windshake, this value of tip/tilt jitter can be achieved with an 18th mag guide star. For NGS AO, this requirement is less severe than the limiting magnitude associated with higher order compensation as plotted in Figure 10, so that tip/tilt compensation is not the limiting factor for sky coverage. For the LGS AO system, the required brightness for the tip/tilt guide star could be reduced by an additional magnitude if windshake could be eliminated entirely. Tip/tilt compensation degrades less rapidly for LGS AO than for NGS AO with increasing tip/tilt guide star magnitude, since the guide star images in the tip/tilt WFS remain compensated by the LGS higher order adaptive optics.

5.3. Sky Coverage

Figure 14 summarizes NGS and LGS AO sky coverage at the Galactic pole for a "nominal" observing scenario with median seeing, a 0° zenith angle, and typical windshake-induced tip/tilt jitter. Sky coverage is described in terms of the probability of achieving a specified Strehl ratio in *J*, *H*, and *K* bands, and analogous results at a Galactic latitude of 30° are plotted in Figure 15. LGS AO provides about a 10-fold increase in sky coverage for a 50% Strehl ratio for all three spectral bands and both guide star density models. The NGS AO system does not suffer from focus anisoplanatism and will provide somewhat higher Strehl ratios for observations very close to very bright guide stars, but the fraction of the sky associated with this performance advantage is on the order of 0.001–0.003. The fractional sky coverage asymptotes to a value less than unity at a low Strehl ratio because there is a nonzero probability that absolutely no guide stars will be found within the 2′ field of view of the Gemini WFSs.

Figures 16 and 17 illustrate the effects of seeing and zenith angle upon AO system sky coverage in the *H* band. Good seeing increases the probability of a 50% Strehl ratio from 2% to 9% with NGS AO, and from 35% to 70% with LGS AO. Observing at a 45° zenith angle reduces these probabilities to 0.5% and 8%, respectively. Scheduling algorithms for queue-based observing will need to account for these variations to maximize the benefits obtained from either AO system option.

The effects of AO conjugate range and windshake on sky coverage are plotted in Figures 18 and 19, respectively. Changing the AO conjugate range from 0.0 to 6.5 km increases the probability of a 50% Strehl in the *H* band by at least a factor of 2 for both NGS and LGS AO systems. The severe windshake model decreases this measure of sky coverage by about a factor of 2 relative to typical windshake, while the improvements obtained by eliminating windshake entirely are relatively modest.

6. SUMMARY

We have described an approach to evaluating the sky coverage achieved by an astronomical adaptive optics system and have presented sample results for several NGS and LGS AO configurations using scenario, telescope, and AO design parameters derived from the Gemini-North 8 m telescope. With "sky coverage" defined as the fraction of the sky for which the AO system provides a high Strehl ratio in the *J*, *H*, or *K* band, LGS AO using a single beacon in the mesospheric sodium layer typically improves sky coverage by about an order of magnitude relative to NGS AO. These results account for many factors of special significance for Gemini-North, including Mauna Kea turbulence profiles, tip/tilt jitter induced by ground-level winds (windshake), wavefront sensing and correction optically conjugate to a range of 6.5 km, and partial compensation of the tip/tilt guide star image by the higher order adaptive optics. This last factor is particularly important for LGS AO, since a very dim natural guide star may be used for tip/tilt sensing when its image is sharpened by LGS higher order compensation.

The values assumed for windshake, seeing, zenith angle, and the conjugate range of the adaptive optics have highly important effects upon sky coverage for both LGS and NGS AO systems. Changing the AO conjugate range from 6.5 km to the telescope primary mirror reduces sky coverage by about a factor of 3 for LGS AO and a factor of 2 for NGS AO. Changes in seeing due

to either atmospheric turbulence or the choice of zenith angle can increase or decrease sky coverage by a factor of 3 or 4. The severity of windshake largely determines the required tip/tilt control bandwidth and sampling rate, thereby defining the necessary tip/tilt guide star magnitude and influencing sky coverage to a similar degree. These last three factors must be considered by any efficient scheduling algorithm for queue-based observing.

A more general observation from this study is that the results of a very wide range of AO system design decisions may be evaluated directly in terms of their impact upon sky coverage using equations (4.1) and (4.2) above once the Strehl ratio function $S(\theta, R, c)$ has been calculated. Similar sky coverage results may be computed in terms appropriate for particular scientific instruments (e.g., fractional slit throughput for a spectrometer), once parameters such as pixel subtense, slit width, and the instrument's optical transfer function are specified. Evaluating AO system performance in terms related as closely as possible to specific scientific applications will improve the probability of effective design decisions and increase the chances that realistic expectations will be met.

We are grateful to D. Simons, J. Oschmann, R. McGonegal, and F. Gillett for specifying the observing scenarios and system parameters to be used for this analysis. R. Racine provided guidance on the interpretation of Mauna Kea turbulence profiles. An anonymous reviewer supplied many helpful comments and suggestions on the first draft of the manuscript. This study was funded by the Air Force Office of Scientific Research. The authors gratefully acknowledge their support.

APPENDIX

RADIOMETRY FORMULAE

This appendix summarizes the first-order formulae for WFS radiometry and tip/tilt measurement accuracy used in this analysis. This noise model is one of three terms that must be specified to evaluate the performance of an AO system, the other two being a statistical description of atmospheric turbulence and a linear systems model for the AO system itself. Our approach to modeling these latter quantities is described elsewhere (Ellerbroek 1994).

The rms one-axis tip/tilt measurement error for a single subaperture in a Shack-Hartmann WFS can be described by the formula

$$\sigma_\theta = \frac{\theta_B}{\mathrm{SNR}}, \tag{A1}$$

where θ_B is the effective spot size for the guide star image (or "blur") $B(r)$ in the focal plane of the WFS, and SNR is the total signal–to–rms noise ratio for a single subaperture image. SNR may vary from subaperture to subaperture owing to edge effects, and θ_B may vary between subapertures as well as within a subaperture for the x- and y-tilt measurements. For quadrant detector tilt sensing, the SNR is given by

$$\mathrm{SNR} = \frac{N_p}{\sqrt{N_p + 4N_b + 4\sigma_e^2}}, \tag{A2}$$

where N_p is the number of signal photodetection events per subaperture, N_b is the number of background photodetection events per pixel, and σ_e is the rms detector read noise per pixel per frame.

For a natural guide star, the signal level N_p is computed as

$$N_p = z10^{-m/2.5}10^{-(\sec\psi - 1)M_a/2.5}\tau tA, \tag{A3}$$

where z is the intensity of a zero-magnitude guide star at the top of the atmosphere, m is the guide star magnitude, ψ is the zenith angle, M_a is the atmospheric attenuation in magnitudes per air mass, τ is the end-to-end efficiency of the telescope optics and WFS detectors, t is the integration time, and A is the area of the WFS subaperture in the telescope aperture plane. For a laser guide star, N_p is described by the formula

$$N_p = z'p10^{-2(\sec\psi - 1)M_a/2.5}\cos\psi\tau tA, \tag{A4}$$

where z' is the guide star intensity in the aperture plane of the telescope for a 1 W illuminator laser, p is the illuminator laser power in watts, and the remaining variables are defined as for the natural guide star case. This formula neglects the effects of saturation in the mesospheric sodium layer which occur at very high illuminator powers. A factor $2(\sec\psi - 1)$ occurs in the

exponent because two-way atmospheric transmittance losses must be accounted for, but these losses are already included in the measured value of z' for the case $\psi = 0^\circ$. Although the solid angle subtended by a WFS subaperture relative to the laser guide star varies as $(\cos\psi)^2$, the effective column density of the sodium layer increases as $(\cos\psi)^{-1}$ until ψ approaches $\pi/2$. These two competing effects yield the $\cos\psi$ term appearing in equation (A4).

The background signal level per pixel level is given by

$$N_b = z_b \tau t A w^2, \tag{A5}$$

where z_b is the background intensity per square arcsecond in the plane of the telescope, w is the angular subtense of a WFS pixel, and τ, t, and A are as defined above. Variations in the background level with zenith angle have not been considered.

For quadrant detector tilt sensing, the effective guide star spot size for the x-tilt measurement is described by the formula (Tyler & Fried 1982; Welsh et al. 1995)

$$\theta_B = \frac{\int_{\lambda_1}^{\lambda_2} d\lambda I(\lambda)}{4 \int_{\lambda_1}^{\lambda_2} d\lambda I(\lambda) \int_0^\infty d\kappa \hat{B}(\kappa, 0; \lambda)}, \tag{A6}$$

where $[\lambda_1, \lambda_2]$ is the WFS spectral passband, $I(\lambda)$ is the measured source spectrum described in terms of photodetection events per nanometer, $B(\boldsymbol{r}; \lambda)$ is the short-exposure, noise-free guide star image at wavelength λ, and $\hat{B}$ is the Fourier transform of this image. θ_B is the reciprocal of the on-null value of the slope of the transfer curve that describes the normalized energy imbalance between the right- and left-hand sides of the quadrant detector as a function of the subaperture wavefront tilt. For the y-tilt measurement, $\hat{B}(\kappa, 0; \lambda)$ must be replaced by $\hat{B}(0, \kappa; \lambda)$. For a natural guide star or a laser guide star smaller than the isoplanatic angle, $\hat{B}(\boldsymbol{\kappa}; \lambda)$ is described by the equation

$$\hat{B}(\boldsymbol{\kappa}; \lambda) = \hat{G}(\boldsymbol{\kappa}; \lambda) \mathrm{OTF}(\boldsymbol{\kappa}; \lambda), \tag{A7}$$

where $\hat{G}$ is the Fourier transform of the guide star intensity distribution ($\equiv 1$ for the NGS case), and OTF is the mean optical transfer function of the subaperture. Neglecting scintillation effects, this latter function may be computed as

$$\mathrm{OTF}(\boldsymbol{\kappa}; \lambda) = \left[\int d\boldsymbol{r} W(\boldsymbol{r})\right]^{-1} \int d\boldsymbol{r} W(\boldsymbol{r}) W(\boldsymbol{r} - \lambda\boldsymbol{\kappa}) \exp\left\{-\frac{1}{2}\left(\frac{2\pi}{\lambda}\right)^2 \left\langle [\mathrm{OPD}(\boldsymbol{r}) - \mathrm{OPD}(\boldsymbol{r} - \lambda\boldsymbol{\kappa})]^2 \right\rangle\right\} . \tag{A8}$$

Here $\boldsymbol{r}$ denotes coordinates in the telescope aperture plane, $W(\boldsymbol{r})$ is a $\{0, 1\}$-valued function defining the WFS subaperture, $\mathrm{OPD}(\boldsymbol{r})$ is the tilt-removed residual optical path difference after compensation by the higher order adaptive optics, and the angle brackets denote ensemble averaging over WFS noise and atmospheric turbulence statistics. For the large subapertures in the Gemini-North tip/tilt WFS, equation (A8) must be evaluated numerically to assess the degree of sharpening of the tip/tilt guide star image achieved by the higher order adaptive optics. For the small, square subapertures in the higher order WFS, equation (A8) is estimated using the Fried approximation for the short-exposure OTF (Fried 1966):

$$\mathrm{OTF}(\boldsymbol{\kappa}; \lambda) = \mathrm{OTF}_{\mathrm{DL}}(\boldsymbol{\kappa}; \lambda) \mathrm{OTF}_A(\boldsymbol{\kappa}; \lambda), \tag{A9}$$

$$\mathrm{OTF}_{\mathrm{DL}}(\kappa, 0; \lambda) = \begin{cases} 1 - \left(\dfrac{\kappa\lambda}{w}\right) & \text{if } \kappa \le w/\lambda, \\ 0 & \text{otherwise;} \end{cases} \tag{A10}$$

$$\mathrm{OTF}_A(\kappa, 0; \lambda) = \begin{cases} \exp\left\{-3.44 \left(\dfrac{\kappa\lambda}{r_0}\right)^{5/3} \left[1 - \left(\dfrac{\kappa\lambda}{w}\right)^{1/3}\right]\right\} & \text{if } \kappa \le w/\lambda, \\ 0 & \text{otherwise.} \end{cases} \tag{A11}$$

Here w is the width of a subaperture, $\mathrm{OTF}_{\mathrm{DL}}$ is the diffraction-limited OTF for a WFS subaperture, and OTF_A is a transfer function approximation to the effect of uncompensated atmospheric turbulence upon short-exposure imaging. Equation (A11) neglects the fact that the subapertures are square, not circular, and equation (A10) is also an approximation for the partial subapertures at the edge of the WFS pupil.

The most probable approach to projecting a laser guide star for Gemini would employ a separate, relatively small launch telescope

without atmospheric turbulence compensation. In analogy to equations (A9)–(A11), the Fourier transform of the laser guide star intensity distribution is approximated as

$$\hat{G}(\boldsymbol{\kappa};\lambda) = \hat{G}_{\rm DL}(\boldsymbol{\kappa};\lambda)\hat{G}_A(\boldsymbol{\kappa};\lambda), \tag{A12}$$

$$\hat{G}_{\rm DL}(\kappa, 0;\lambda) = \begin{cases} \left(\frac{2}{\pi}\right)\left[\cos^{-1}\left(\frac{\kappa\lambda}{D_T}\right) + \left(\frac{\kappa\lambda}{D_T}\right)\sqrt{1-\left(\frac{\kappa\lambda}{D_T}\right)^2}\right] & \text{if } \kappa \le D_T/\lambda, \\ 0 & \text{otherwise;} \end{cases} \tag{A13}$$

$$\hat{G}_A(\kappa, 0;\lambda) = \begin{cases} \exp\left\{-3.44\left(\frac{\kappa\lambda}{r_0}\right)^{5/3}\left[1-\left(\frac{\kappa\lambda}{D_T}\right)^{1/3}\right]\right\} & \text{if } \kappa \le D_T/\lambda, \\ 0 & \text{otherwise.} \end{cases} \tag{A14}$$

D_T is the aperture diameter of the circular laser launch telescope, and $\hat{G}_{\rm DL}$ and $\hat{G}_A$ are the contributions to the guide star intensity profile due to diffraction and atmospheric turbulence effects. Equations (A12)–(A14) ignore the effects of (1) aberrations in the illuminator laser and the launch telescope, (2) the spread in the LGS intensity distribution due to the depth of the sodium layer, and (3) any correlation in atmospheric turbulence between the laser launch telescope and the Gemini aperture.

Finally, the overall tip/tilt measurement is computed from the outputs of the four subapertures in the tip/tilt WFS as the average

$$\theta = \frac{\sum_i A_i\theta(i)}{\sum_i A_i}, \tag{A15}$$

where A_i is the illuminated area of subaperture number i. These areas will vary for the LGS AO case with an off-axis tip/tilt guide star when the WFS entrance pupil is not optically conjugate to the telescope primary mirror. Since the WFS measurement noise is uncorrelated between subapertures, the rms noise in the overall tip/tilt measurement can be evaluated using the expression

$$\sigma_\theta = \frac{\left(\sum_i A_i^2\sigma_{\theta(i)}^2\right)^{1/2}}{\sum_i A_i}, \tag{A16}$$

where $\sigma_{\theta(i)}$ is the rms tip/tilt measurement error for subaperture number i. For the LGS AO case, $\sigma_{\theta(i)}$ may be different for the x- and y-tilt measurements because the images of an off-axis tip/tilt guide star will be elongated owing to anisoplanatism.

REFERENCES

Avicola, K., et al. 1994, J. Opt. Soc. Am. A, 11, 825
Bahcall, J. N., & Soneira, R. M. 1980, ApJS, 44, 73
Bely, P. 1987, PASP, 99, 560.
Close, L. M., Roddier, F., Roddier, C., Northcott, M., & Graves, J. E. 1996, in Adaptive Optics, ed. P. Wizinowich & B. Welsh (Washington, DC: Opt. Soc. Am), 112
Ellerbroek, B. L. 1994, J. Opt. Soc. Am. A, 11, 783
Ellerbroek, B. L., Van Loan, C., Pitsianis, N. P., & Plemmons, R. J. 1994, J. Opt. Soc. Am. A, 11, 2871
Fried, D. L. 1966, J. Opt. Soc. Am., 56, 1372
———. 1982, J. Opt. Soc. Am., 72, 52
Morris, S. et al. 1996, Science Drivers for Adaptive Optics on Gemini-North (Gemini document RPT-PS-G0069)
Olivier, S. S., Max, C. E., Gavel, D. T., & Brase, J. M. 1993, ApJ, 407, 428
Oschmann, J. 1995, Gemini document TN-S-G0035
Parenti, R. R., & Sasiela, R. J. 1994, J. Opt. Soc. Am. A, 11, 288
Racine, R., & Ellerbroek, B. L. 1995, in Adaptive Optical Systems and Applications, ed. R. K. Tyson & R. Q. Fugate (Bellingham: SPIE), 248
Racine, R., Salmon, D., Cowley, D., & Sovka, J. 1991, PASP, 103, 1020
Rigaut, F., Ellerbroek, B. L., & Northcott, M. 1997, Appl. Opt., 36, 2856
Rigaut, F., & Gendron, E. 1992, in Laser Guide Star Adaptive Optics Workshop, ed. R. Fugate (Albuquerque: Starfire Optical Range), 582
Rigaut, F., Lena, P., Madec, P. Y., Rousset, G., Gendron, E., & Merkle, F. 1992, in Progress in Telescope and Instrumentation Technologies, ed. M.-H. Ulrich (Garching: ESO), 399
Rigaut, F., et al. 1996, in Adaptive Optics, ed. P. Wizinowich & B. Welsh (Washington, DC: Opt. Soc. Am), 46
Roddier, F. 1992, Report on the Seeing on Mauna Kea (Univ. of Hawaii)
Ryan, P. T., Angel, J. R. P., McCarthy, D. W., Close, L. M., Mohanty, S., Fugate, R., & Sandler, D. G. 1996, in Adaptive Optics, ed. P. Wizinowich & B. Welsh (Washington: Opt. Soc. Am), 118
Shelton, J. C., Schneider, T. G., McKenna, D., & Baliunas, S. L. 1996, in Adaptive Optics, ed. P. Wizinowich & B. Welsh (Washington: Opt. Soc. Am.), 43
Tyler, D. W., & Ellerbroek, B. L. 1998, Appl. Opt., in press
Tyler, G. A., & Fried, D. L. 1982, J. Opt. Soc. Am., 72, 804
Welsh, B. M., Ellerbroek, B. L., Roggemann, M. C., & Pennington, T. L. 1995, in Adaptive Optical Systems and Applications, ed. R. K. Tyson & R. Q. Fugate (Bellingham: SPIE), 277